Paper No.
4868

Characterization of Oxide Layers Formed During Corrosion in Supercritical Water

A.T.Motta[1], J.Bischoff[1], A. Siwy[1] and M.J. Gomes da Silva[1]
[1]*Department of Mechanical and Nuclear Engineering, 227 Reber Building, Pennsylvania State University, University Park, PA, 16802.*

R.J. Comstock[2]
[2]*Westinghouse Electric Co., Science and Technology Department, 1340 Beulah Road Pittsburgh, PA 15235*

Z. Cai[3] and B.Lai[3]
[3]*Advanced Photon Source, Argonne National Laboratory, Argonne, IL, 60439, USA*

Contact email: atm2@psu.edu

ABSTRACT

The Supercritical Water Reactor is one of the Generation IV nuclear power plant designs envisioned for its high thermal efficiency. Uniform corrosion is one of the main challenges to finding suitable materials for structural components and fuel cladding. The corrosion rate depends on the nature of the protective oxide formed, such that small alloying content differences cause significant differences in corrosion rate. By studying in detail the oxide layer with a combination of microbeam synchrotron radiation diffraction and fluorescence and transmission electron microscopy, it is possible to discern which characteristic oxide structures lead to protective behavior and a lower corrosion rate.

A review is presented of studies conducted in protective oxide layers formed during corrosion of zirconium alloys and in ferritic-martensitic and oxide dispersion strengthened steels in supercritical water at 500-600 C for different exposure times. Microbeam synchrotron radiation diffraction and fluorescence allows us to probe the structure of the oxide layers with unprecedented sensitivity and sub-micron spatial resolution. For the zirconium alloys a characteristic structure formed at the oxide-metal interface is associated with protective behavior. In the case of advanced steels, a sequence of sub layers of oxide layers is observed where particular phases are shown to be crucial to protective behavior.

INTRODUCTION

The Supercritical Water Reactor is one of the Generation IV nuclear power plant designs envisioned for its high thermal efficiency and plant simplification [1]. Supercritical water at 500ºC and 600ºC (where the reactor is designed to operate) represents a very corrosive environment. Consequently, resistance to uniform corrosion is a key requirement for the candidate alloys envisioned as cladding or structural materials. The corrosion behavior of an alloy depends strongly on the structure of the protective oxide formed on the alloy. Therefore by understanding the nature of these oxide microstructures it is possible to determine the reasons for their protective behavior.

A brief illustration is presented of the application of advanced characterization techniques for the study of oxide growth in steels and in zirconium alloys during exposure to supercritical water. A very useful technique for a detailed analysis of the oxide microstructure is microbeam synchrotron radiation diffraction and fluorescence. This has been used to characterize the oxide layers formed on ferritic-martensitic and zirconium alloys [2, 3]. In addition, cross-sectional transmission electron microscopy of oxide samples prepared using focused ion beam has been used to further characterize these oxides [2, 4, 5]. This article reviews the studies conducted to characterize the oxide structure formed on these alloys to discern the alloy corrosion protection mechanisms in supercritical water.

EXPERIMENTAL PROCEDURES

Materials

The two ferritic-martensitic alloys studied are 9CrODS and HCM12A. These alloys were both exposed to 500 and 600ºC supercritical water in the corrosion loop at the University of Wisconsin. 9CrODS is an oxide dispersion strengthened steel alloy containing a fine uniform dispersion of Y_2O_3 nano-particles that was mechanically alloyed, normalized at 1050ºC for one hour, air-cooled and then tempered at 800ºC for another hour [6]. This sample was supplied by Japan Atomic Energy Agency to the University of Wisconsin. HCM12A is a generation three ferritic-martensitic alloy that was normalized at 1050ºC for one hour and then tempered at 770ºC for seven hours. Both alloys were corroded in supercritical water at 500ºC and 600ºC and a pressure of 25 MPa for 2, 4 and 6 weeks. The zirconium alloys studied were model Zr-Fe-Cr alloys that were corroded in supercritical water at the dynamic corrosion loop at the University of Michigan at 500ºC and 24.1 MPa where the conductivity, the oxygen content and flow rate were monitored [7]. These samples were corroded for up to 400 days [3]. These samples were also corroded in 500ºC steam at Westinghouse in a static autoclave at 10.34 MPa. Note that the distinction between steam and supercritical water is made because of the lower pressure when using the former than when using the latter. Samples were prepared from the corroded coupons for examination in the synchrotron facility and for transmission electron microscopy examination, using procedures previously described [2, 8].

Synchrotron radiation

Microbeam synchrotron X-ray diffraction and fluorescence was performed at the 2-ID-D beamline of the Advanced Photon Source at Argonne National Laboratory, in which the incident beam can be focused to a 0.2 micron spot with energy of 9.5 keV. Figure 1 shows the experimental geometry at the beamline. The incident beam angle used (16 degrees) creates a footprint on the sample of about 0.2 x 2 μm^2. Both diffraction and fluorescence information are acquired simultaneously at each spot.

Consequently, the whole oxide layer is scanned spot by spot to obtain the diffraction patterns (which when the peaks are indexed give a "map" of the phases present) and elemental composition of the oxide.

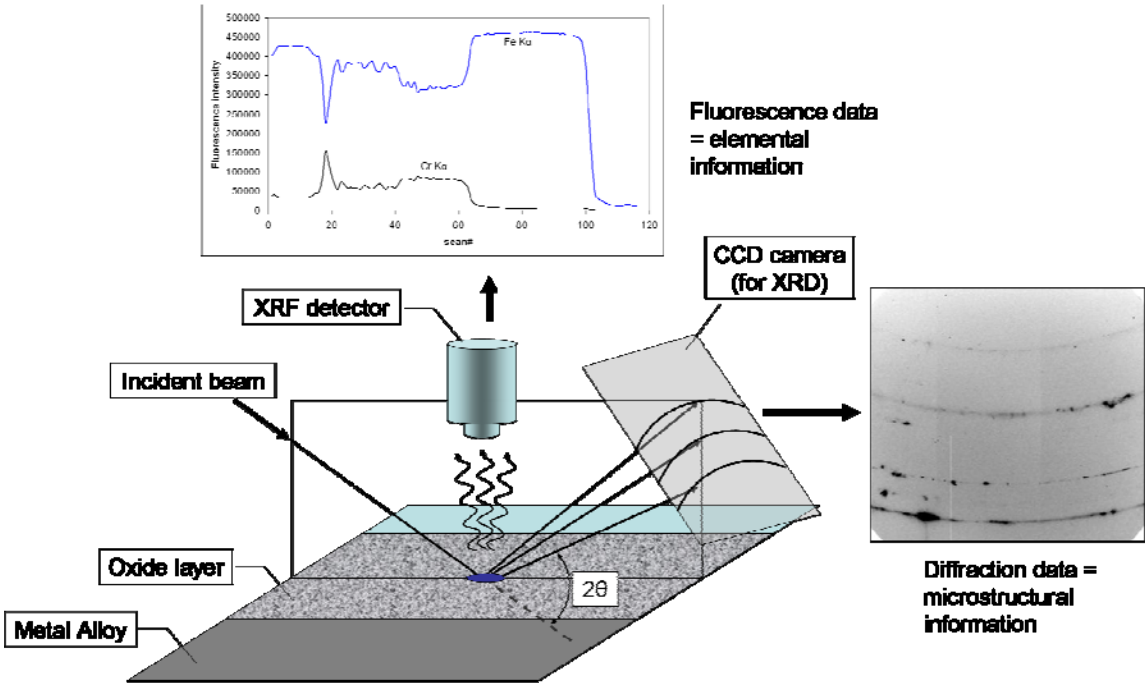

Figure 1 - Diffraction geometry for microbeam synchrotron radiation diffraction and fluorescence experiments [9].

The integrated diffraction patterns were fit using PeakFit [10] to determine the location and area of the peaks. The high resolution of the synchrotron radiation facility enables us to differentiate between Fe_3O_4 and $FeCr_2O_4$ phases, which have the same crystal structure and similar cell parameters.

Electron Microscopy

The samples were examined using electron microscopy. Transmission Electron Microscopy (TEM) samples were prepared with a FEI Company Quanta 200 3D Dual Beam Focused Ion Beam (FIB), using a modified version of the lift-out method. In our case, the specimen was lifted from the bulk substrate first and then thinned to electron transparency. TEM images were obtained using a Philips 420 instrument operated at 120 keV.

RESULTS AND DISCUSSION

Since the objective of this work is to show the relation between corrosion kinetics and oxide microstructure, the corrosion kinetics during testing in supercritical water and as measured by the corrosion weight gain are shown in Figure 2. Samples from these tests that were archived at various times were examined using microbeam synchrotron radiation diffraction and fluorescence as described in the following.

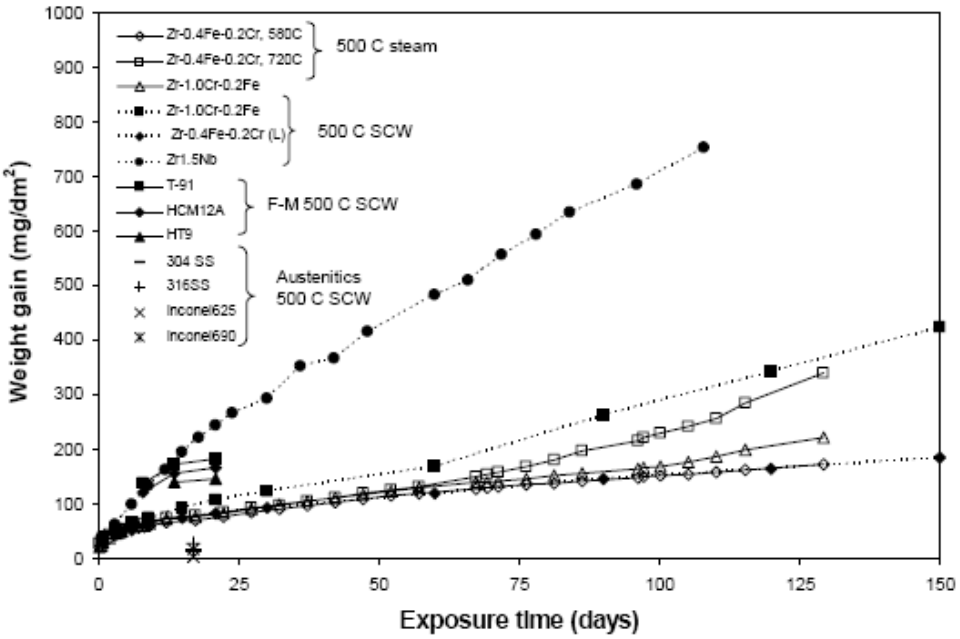

Figure 2: Weight gain versus exposure times for various alloys of interest to the supercritical water reactor. [3]

9CrODS steel

Figure 3(a,d) shows SEM images of the oxide layers formed on 9CrODS corroded at 600ºC for 2 and 4 weeks. The oxidation of ferritic-martensitic alloys in supercritical water at 600ºC creates a three-layer oxide structure, with many sub-layers. The outer layer is formed by outward migration of Fe and is thought to be porous and formed of large grains of Fe_3O_4. The inner layer shows a mixture of $FeCr_2O_4$ and Fe_3O_4 with the former being more prevalent near the interface with the diffusion layer. The diffusion layer contains a mixture of metal grains and oxide precipitates ($FeCr_2O_4$ and Cr_2O_3). It is not clear from the pictures which layer or sub-layer is the barrier layer, (the layer that provides protection by forcing oxidizing species to be transported through it by solid state diffusion), but some discussion on the identification of the barrier layer is given later in the paper.

These samples were examined using microbeam synchrotron radiation. Figure 3(b,e) shows the x-ray fluorescence spectra from the scan of these oxides. Figure 3(c,f) shows two diffraction patterns taken at the points indicated. The fit of the diffraction patterns shown in Fig. 3(c,f) indicates the presence of Cr_2O_3 at the two circled locations (inner part of the inner layer after 2 weeks and the inner part of the diffusion layer after 4 weeks).

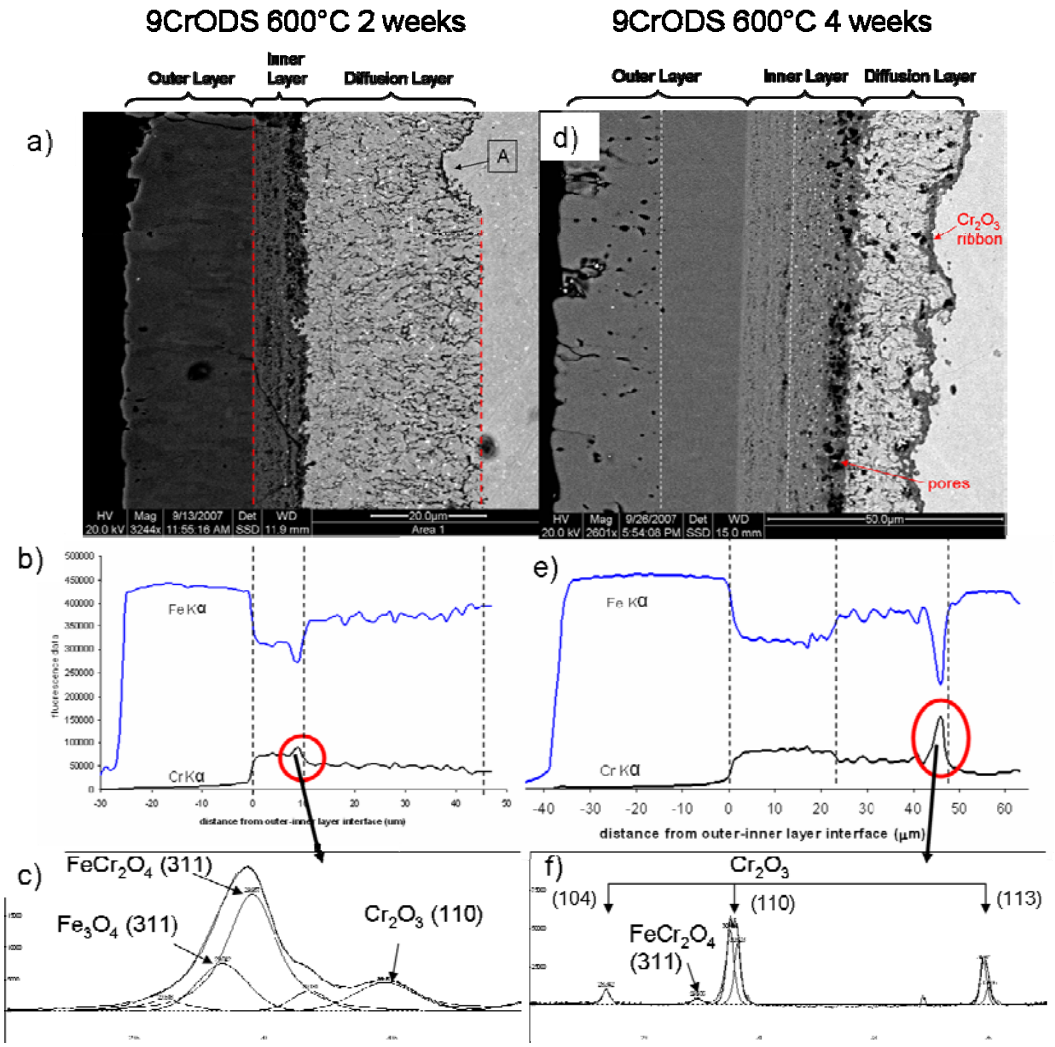

Figure 3 - SEM and microbeam synchrotron radiation fluorescence and diffraction data for 9CrODS 600ºC 2 and 4 week samples. a) and d) are SEM images, b) and e) fluorescence plots and c) and f) magnifications of diffraction patterns taken at the location of chromium enrichment.

The SEM images show that there is significant change in oxide structure between the 2 week and 4 week sample. In the 2 week sample, the inner oxide is thin compared to the diffusion layer. A slight chromium enrichment is observed at the inner oxide-diffusion layer interface, matching the observation of peaks associated with Cr_2O_3 at this location. In the 4 week sample on the other hand, a relatively thick and continuous oxide ribbon has formed at the diffusion layer metal interface which appears to inhibit further oxidation of the metal. As the diffraction data shows in Figure 3(f), this oxide ribbon is mainly composed of Cr_2O_3 which may explain the absence of oxidation beyond this interface. In the SEM image of 9CrODS 600ºC 2 weeks of Figure 3(a) we can observe the beginning of the formation of the Cr_2O_3 ribbon at the region marked "A".

Figure 4 shows the microbeam X-Ray diffraction data for the examination of the oxide layer formed on the 9CrODS 600ºC sample after a four week exposure.

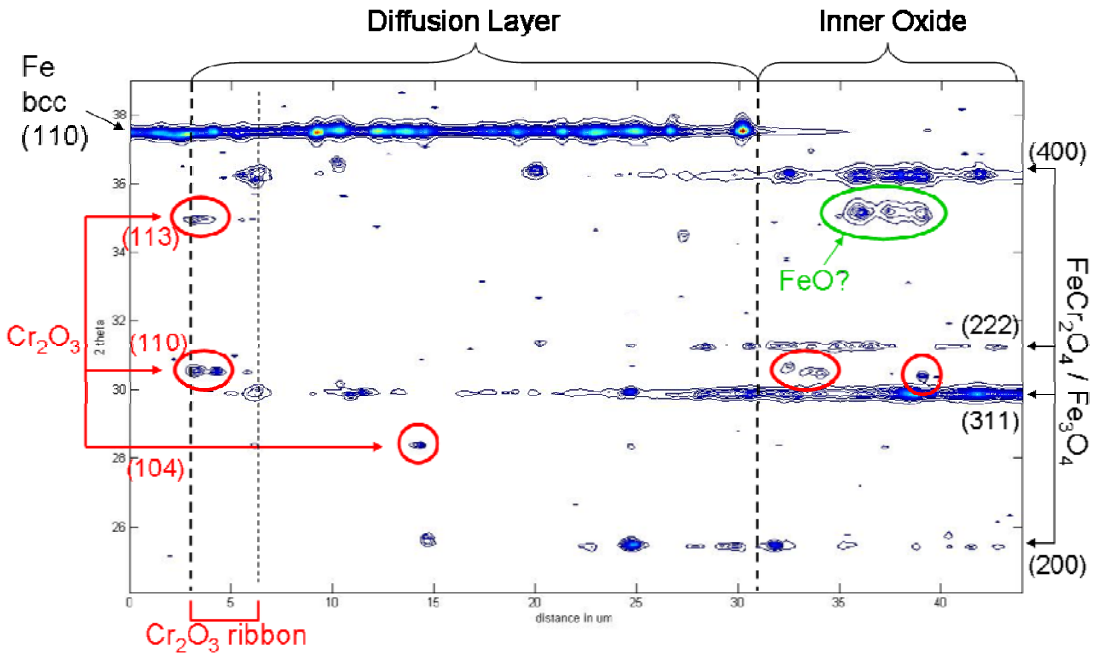

Figure 4 - Microbeam synchrotron radiation diffraction data for oxide layer formed on 9CrODS after exposure to 600ºC supercritical water for 4 weeks[9]

The diffraction plot of Figure 4 shows the diffraction peaks observed throughout the diffusion layer and part of the inner oxide. The Cr_2O_3 ribbon is distinct with strong Cr_2O_3 (110) and (113) peaks. This plot also shows that the ribbon is actually divided into two regions, one containing Cr_2O_3 near the metal and one containing mostly $FeCr_2O_4$. Additionally, Cr_2O_3 is observed at the inner oxide-diffusion layer interface as was the case in the 2 week sample. Slightly further in the inner oxide, peaks possibly associated with FeO are observed which were not seen in the 2 week sample. The appearance of this phase might be due to the shift of the chromium enrichment from the inner oxide-diffusion layer interface to the diffusion layer-metal interface.

These structures were further characterized using transmission electron microscopy. The focused ion beam technique allowed the production of cross sectional samples with large imaging area from precise locations within the oxide layer.

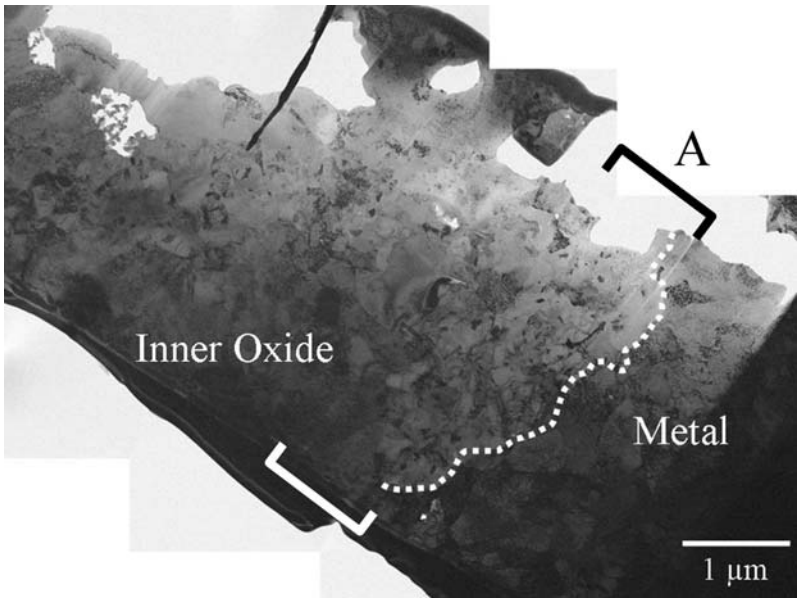

Figure 5: Bright field transmission electron micrograph of the diffusion layer-metal interface for 9CrODS sample after exposure to 600ºC for 4 weeks.[5]

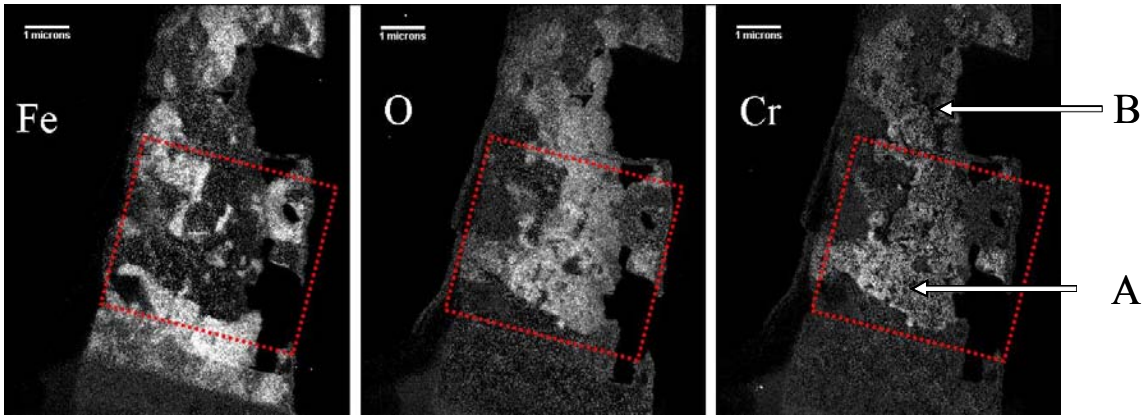

Figure 6: Energy Filtered images Fe, Cr and O taken from the diffusion layer-metal interface in 9CrODS corroded in 600ºC supercritical water for 4 weeks [5].

Figure 5 shows a bright field image of the diffusion layer/metal interface. The light band at the interface and marked as region "A" was found to be Cr-rich, as shown later by energy filtered imaging using EELS analysis. Tilting this sample revealed that the light band along the diffusion layer/metal interface consists of either large irregularly shaped grains or large areas of grouped grains which could be highly oriented. These shapes are better shown in the energy filtered EELS maps of iron, oxygen, and chromium for this shown in Figure 6. A strong correlation of chromium and oxygen within the diffusion layer can be seen in the elemental maps.

HCM12A

Further evidence of the relationship between oxide growth and metal microstructure is shown in Figure 7, which consists of two SEM images of HCM12A corroded at 600ºC for 2 weeks: a low magnification view of the whole oxide layer and a magnification of the inner and diffusion layers. HCM12A does not have the same microstructure as 9CrODS because it does not contain the nano-ODS particles and it

exhibits ferritic-martensitic laths outlined by white lines in the SEM image. Although the base metal microstructure is different, both alloys show similar oxidation behavior with a three-layer structure containing Fe_3O_4 in the outer oxide, a mixture of $FeCr_2O_4$ and Fe_3O_4 in the inner oxide, and a diffusion layer containing a mixture of oxide precipitates ($FeCr_2O_4$ and Cr_2O_3) and Fe bcc metal grains. The oxidation of HCM12A stands out from that of 9CrODS in clear correlation of the base metal microstructure with the oxide precipitation observed in the diffusion layer. This is shown by the close-up SEM image of the inner and diffusion layers. In this image the oxide precipitates are visible as aligned along the white lines outlining the ferritic-martensitic laths boundaries and prior austenite grain boundaries.

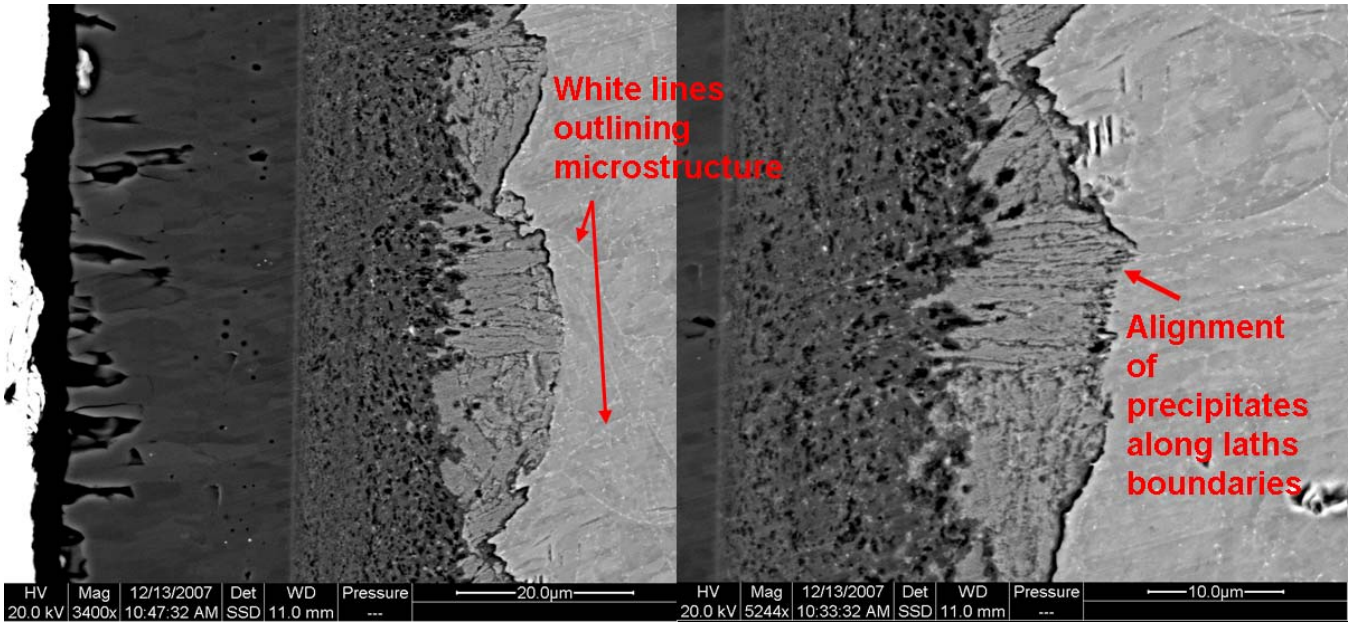

Figure 7: Scanning electron micrographs of an oxide layer formed in HCM12A after exposure to supercritical water at 600ºC for 2 weeks.

Zirconium alloys

Zirconium alloys, widely used for nuclear fuel cladding, exhibit significant variations in corrosion behavior with small changes in alloying element composition during corrosion testing in 360ºC water. These manifest themselves as variations in both the pre-transition oxide growth rate and on the rate of loss of protectiveness (oxide transition). This has been well established for corrosion in water, whereas corrosion in supercritical water at the 500-550ºC temperature expected to be present in a SCWR has received less attention.

Zirconium alloys initially did not receive much consideration for these high temperature applications because it was thought that the corrosion rates would be too high, and that the materials would not be strong enough. However earlier work [11-13] indicated that some high alloying content Zr alloys showed promise for high temperature corrosion applications. There are significant advantages associated with using a more neutron-transparent cladding material than the alloys currently envisaged for the SCWR (Inconels and steels), including decreasing the required fuel enrichment and greater core design flexibility. Thus, as part of a research program to assess the corrosion behavior of Zr alloys under supercritical water (SCW), we have performed extensive corrosion testing of model Zr alloys under

SCW, followed by oxide characterization using microbeam synchrotron radiation diffraction and fluorescence, as explained above.

Figure 8 shows the diffracted intensity versus two-theta plots arranged as a function of distance from the oxide-metal interface. The peaks for the different phases are labeled. In the metal region, three hcp-Zr peaks are present with the 0002Zr basal pole showing low intensity. After the oxide-metal interface, monoclinic ZrO_2 peaks are seen. The differences between the microstructure of protective and nonprotective oxides were most apparent at the oxide-metal interface. Figure 8(a) taken from an oxide layer formed on alloy Zr-0.2Fe-0.1Cr (H) during corrosion in water at 360°C illustrates the structure of a protective oxide. In particular, the peak shown at 28.7 degrees is present in the protective oxides, and absent in the nonprotective oxide layers. This peak has been identified previously as the 002t peak, belonging to a highly oriented tetragonal phase forming at the interface [14]. As discussed below, the orientation relationships of this peak both with the metal and with the monoclinic phase into which it transforms suggest that this phase is a "precursor" phase, the presence of which allows the monoclinic phase to form in a more oriented fashion, and in a manner that minimizes stress accumulation in the oxide. This reduces the tendency for oxide breakup and loss of protective behavior.

This oxide-metal interface structure was also present in the oxide layers formed at 500°C, both in steam and in supercritical water. However, the intensity of the 002t peak was much more prominent in the oxide formed at 500°C than in the oxides formed at 360°C. Figure 8(b) shows a plot of diffracted intensity versus two-theta angle versus position in the oxide layer for a scan conducted on an oxide layer formed on Zr-0.2Fe-0.1Cr (H) after 150 days of exposure in supercritical water. This alloy maintains protective oxide growth in supercritical water up to 150 days. As can be seen, the 002t peak forms at the interface, with a much higher intensity than that of the same peak formed in 360°C water corrosion in the same alloy. For all non protective oxides studied, no interfacial phases are seen. The fact that the same oxide-metal interface structures are present in protective oxide layers formed during exposure to 360°C water and in 500°C steam or supercritical water indicates that similar mechanisms for forming protective oxides are present at both temperatures**.**

The layers present at the oxide metal interface in both Fe-Cr and Zr alloy systems appear to control the corrosion behavior and are associated with the overall protective oxide behavior. The study of these layers especially when correlated with the microstructure of the metal can provide clues as to how good alloy design increases alloy protectiveness, especially when combined with complementary information from electron microscopy. To achieve these goals, the spatial resolution, elemental sensitivity, and resolving power of the microbeam synchrotron radiation diffraction and fluorescence make it a powerful tool for studying in detail the structure of growing oxides and thus rationalizing corrosion behavior.

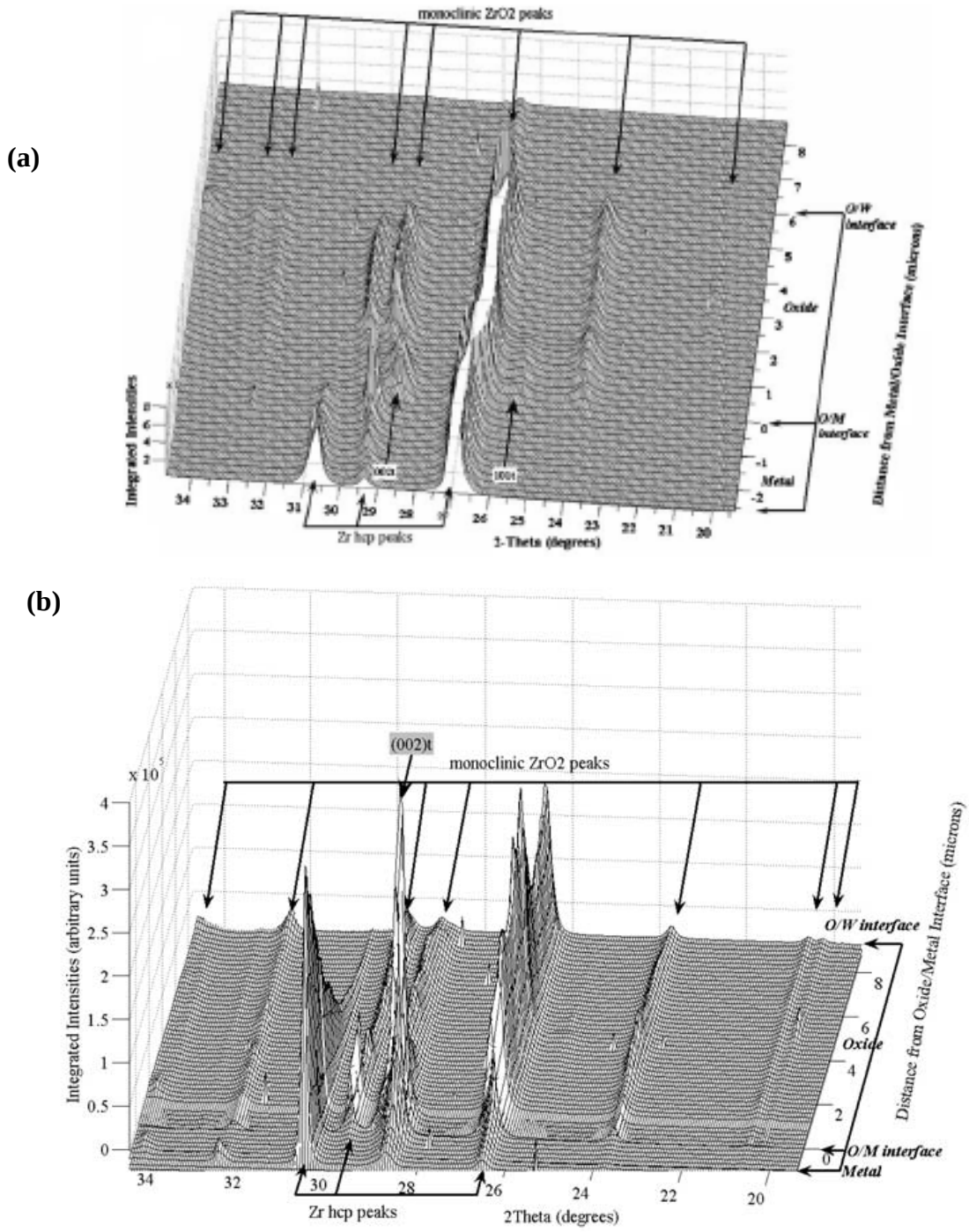

Figure 8: Diffracted intensity versus two-theta angle for various positions in the oxide obtained using microbeam synchrotron radiation diffraction and fluorescence for Zr0.2Fe0.1Cr (H) alloy corroded in (a) 360°C water and (b) 500°C supercritical water [15].

CONCLUSIONS

Oxide layers created during exposure of metallic alloys to supercritical water have been characterized using microbeam synchrotron radiation diffraction and fluorescence and electron microscopy. The main conclusions are as follows.

1. For the oxide dispersion strengthened steel 9CrODS corroded at 600°C, the protection is achieved by the formation of a thin layer of Cr_2O_3 that forms between the second and fourth week of exposure at the interface between the diffusion layer and the base metal.
2. For zirconium alloys corroded in 500°C supercritical water, the protective character of the oxide layer is associated with a highly oriented tetragonal ZrO_2 phase at the oxide-metal interface. This interfacial precursor phase is also present in protective oxides formed in 360°C water, indicating similar protection mechanisms at work.
3. Microbeam synchrotron radiation diffraction and fluorescence can provide structural and chemical information with unique spatial resolution to aid in the understanding of the influence of the base metal in corrosion mechanisms.

ACKNOWLEDGMENTS

The authors would like to thank the JAEA for fabricating the 9CrODS alloy and Todd Allen, and co-workers of the University of Wisconsin-Madison and Gary Was and co-workers at University of Michigan for supplying the corrosion samples used in this study. We also thank T. Clark of Penn State for assistance with energy filtered imaging. Use of the Advanced Photon Source was supported by the U.S. Department of Energy, Basic Energy Sciences, Office of Science, under Contract No. W-31-109-Eng-38. This research was supported by a DOE NERI grant no. DE-FC07-06ID14744.

REFERENCES

[1] "A Technology Roadmap for Generation IV Nuclear Energy Systems," GIF-002-00, 2002.

[2] A. T. Motta, A. D. Siwy, J. M. Kunkle, J. B. Bischoff, R. J. Comstock, Y. Chen, and T. R. Allen, "Microbeam Synchrotron Radiation Diffraction and Fluorescence Study of Oxide Layers formed on 9CrODS Steel in Supercritical Water," *13th Environmental Degradation of Materials in Nuclear Power Plants*, NACE, 2007.

[3] A. Motta, A. Yilmazbayhan, M. Gomes da Silva, R. J. Comstock, G. Was, J. Busby, E. Gartner, Q. Peng, Y. H. Jeong, and J. Y. Park, "Zirconium Alloys for Supercritical Water Reactor Applications: Challenges and Possibilities," *Journal of Nuclear Materials* 371 (2007) 61-75.

[4] A. Yilmazbayhan, E. Breval, A. Motta, and R. Comstock, "Transmission Electron Microscopy Examination of Oxide Layers Formed in Zr Alloys," *Journal of Nuclear Materials* 349 (2006) 265-281.

[5] A. D. Siwy, T. E. Clark, and A. T. Motta, "Transmission Electron Microscopy of oxide development on 9Cr ODS in Supercritical water," *Journal of Nuclear Materials* submitted (2008)

[6] S. Ukai, S. Mizuta, T. Yoshitake, T. Okuda, M. Fujiwara, S. Hagi, and T. Kobayashi, "Tube manufacturing and characterization of oxide dispersion strengthened ferritic steels," *Journal of Nuclear Materials* 283-287 (2000) 702.

[7] Q. Peng, E. Gartner, J. T. Busby, A. T. Motta, and G. S. Was, "Corrosion Behavior of Model Zirconium Alloys in Deaerated Supercritical Water at 500^{o}C," *Corrosion* 63 (2007) 577-590.

[8] A. Yilmazbayhan, A. T. Motta, R. J. Comstock, G. P. Sabol, B. Lai, and Z. Cai, "Structure of Zirconium Alloy Oxides formed in pure water studied with Synchrotron radiation and optical microscopy: relation to corrosion rate," *Journal of Nuclear Materials* 324 (2004) 6-22.

[9] J. B. Bischoff, A. T. Motta, and R. J. Comstock, "Evolution of the Oxide Structure of 9CrODS Exposed to Supercritical Water " *Journal of Nuclear Materials* submitted (2008)

[10] "PeakFit," 4.0 for Windows ed: SPSS Chicago, IL, USA, . 1997.

[11] J. Bolton, "The Corrosion of Zirconium Alloys," in *Corrosion of Reactor Materials II* Vienna: IAEA, 1962, p. 133.

[12] E. Gulbransen and K. F. Andrew, "Oxidation of Zirconium Alloys in Water Vapor Atmospheres Containing Trace Amounts of Oxygen at 375 ° and 575°C," *Electrochemical Technology* 4 (1966) 99.

[13] H. H. Klepfer and D. L. Douglass, "Factors Limiting the Use of Zirconium Alloys in Superheated Steam," ASTM STP, 1964, 118.

[14] A. T. Motta, A. Yilmazbayhan, R. J. Comstock, J. Partezana, G. P. Sabol, Z. Cai., and B. Lai, "Microstructure and Growth Mechanism of Oxide Layers Formed in Zr Alloys Studied with Micro Beam Synchrotron Radiation," *Journal of ASTM International* 2 (2005) Paper # JAI 12375.

[15] A. T. Motta, M. J. G. d. Silva, A. Yilmazbayhan, R. J. Comstock, Z. Cai, and B. Lai, "Microstructural Characterization of Oxides Formed on Model Zr Alloys Using Synchrotron Radiation," *Journal of ASTM International* 5 (2008) paper ID# JAI10125.